Fluid flow-based description of the geometrical features in fluidic channels using the Shannon's information theory: an exploratory study

JOURNAL: Microfluidics and Nanofluidics

Brief Communication

Fluid flow-based description of the geometrical features in fluidic channels using the Shannon's information theory: an exploratory study

S. Ripandelli[1*], D. Pugliese[2*], M. Sotgiu[1], U. Morbiducci[1]

[1]Politecnico di Torino, Department of Mechanical and Aerospace Engineering, 10129 Torino, Italy

[2]Politecnico di Torino, Department of Applied Science and Technology and RU INSTM, 10129 Torino, Italy

*corresponding authors: simone.ripandelli@gmail.com; ORCID: 0000-0001-7867-9461

diego.pugliese@polito.it; ORCID: 0000-0002-6431-1655

Keywords

Shannon Entropy, microfluidics, information theory, thermodynamics, fluids

Abstract

Inspired by Nature, where storing information is an intrinsic ability of natural systems, here we investigate the capability of interacting systems to transport/store the information generated/exchanged in the interaction process in the form of energy or matter, preserving it over time. In detail, here we test the possibility to consider a fluid as a carrier of information, speculating about how to use such information. The final goal is to demonstrate that information theory can be used to illuminate physical observations, even in those cases where the equations describing the phenomenon under investigation are intractable, are affected by a budget of uncertainty that makes their solution not affordable or may not even be known. In this exploratory work an information theory-based approach is applied to microfluidic data. In detail, the classical study of the fluid flow in a microchannel with obstacles of different geometry is faced by integrating fluid mechanics theory with Shannon's theory of information, interpreted in terms of thermodynamics. Technically, computational fluid dynamics simulations at Reynolds' numbers (*Re*) equal to 1 and 50 were carried out in fluidic channels presenting obstacles with rectangular and semicircular shape, and on the simulated flow fields

the Shannon's information theory was applied evaluating the fluid dynamics information entropy content. It emerged that the Shannon Entropy (SE) evaluated at the outflow section of the flow channel depends upon the geometric features (i.e. position, shape, aspect ratio) of the obstacles. This suggests an interpretation of the fluid dynamics establishing in a flow channel presenting obstacles in terms of information theory, that can be used to identify *a posteriori* the geometric features of the obstacles the fluid interacts with. The proposed approach can be applied to flow data at the boundaries of fluid domains of interest to extract information on the process occurring inside a system, do not making any appeal to the governing equations of the phenomenon under observation or intrusive measurements.

1 Introduction

In principle, the behavior of fluids in motion can be fully described by three equations: an equation describing the conservation of mass, a second equation based on the second Newton's law of motion, and a third equation based on the conservation of energy (Cox 2015; Khasanov 2011; Merdasi et al. 2018).

A condition for a real fluid to be in motion is that sufficient energy is to be spent. It follows that the fluid in motion is a system that modifies its internal energy, thus generating a variation

of entropy (S) of the system in a purely thermodynamic meaning. The concept of entropy (not univocally accepted indeed), which can be explained as the level of disorder of a system describing its evolution under the effect of the external environment, was taken up by Claude Shannon in 1948 (Shannon 1948) and applied to the field of information theory in order to describe the level of complexity of a signal in data communication systems. In general, it is still uncommon to apply information theory for the purpose of the analysis of flow fields characterized by different levels of complexity (Ikeda and Matsumoto 1986). Indeed, the idea of considering a fluid in motion as an information carrier is not new, inspired by the fact that Nature uses fluids to transport a plethora of biochemicals. Looking at a fluid in motion as an information carrier (e.g. nutrients to cells, proteins through blood, etc.), a parallelism between fluid flow and information theory based on the definition of the SE can be easily established.

Motivated by the possibility of interpreting a fluid as information carrier, in this study information theory is applied to microfluidics, where its capability to discriminate the shape of obstacles in a channel based on the knowledge of the motion of fluid particles upstream and downstream of the obstacle is tested. In detail, the capability of the SE to discriminate the shape of the obstacle based on the distortion of fluid streamlines is tested, with the final aim to use the SE of the system as a *fingerprint* of the obstacle shape-specific flow perturbation. The

potency of the herein proposed approach has not been largely explored. To cite a valuable example, Pozo et al. (Pozo et al. 2017) analyzed the flow complexity in open systems, approaching the distortion of fluid streamlines in a channel at the level of information transmission.

Technically, here computational fluid dynamics (CFD) solutions of laminar flow in channels presenting obstacles were compared to an "ideal communication" channel where the transmitted and received messages are identical and SE was applied to CFD data. The characterization of microflows as information carriers finds several applications, e.g. to assess mixing efficiency in micromixers (Camesasca et al. 2006; Pennella et al. 2010; Pennella et al. 2012) or in microreactors and in scaffolds and bioreactors for tissue engineering applications (Eijkel and Van den Berg 2005; Bilen and Yapici 2002; Yojina and Ngamsaad 2010; Tariq et al. 2020) and in many other technological fields like solar energy (Ali 2020), nanofluids for manufacturing processes (Wang et al. 2020), heat and mass transfer (Chen et al. 2020; Sajjad et al. 2020; Sözen et al. 2021).

The principal aim of this study, and the reason of its novelty, was to investigate the behavior of a fluid that flows in a channel in presence of obstacle/s characterized by different shape, multiplicity and disposition and employing the information theory. This exploratory study

86 highlights that at defined conditions a simplified approach based on the information theory can

87 be applied to extract information on the processes occurring within closed systems, and that

88 this can be done by measuring only the “information” at systems’ boundaries.

89

2 Methods

In this study a microchannel geometry without and with obstacles of different shape and position was investigated. Overall, as depicted in Fig. 1, nine configurations were considered, i.e. one without obstacles and 8 with obstacles. The ratio between the height of the channel h_{ch} and the characteristic obstacle dimension h_1 was set to $h_1 = h_{ch}/6$. In microchannel configurations where more than one obstacle was considered, inter-distance was set equal to $h_{ch}/2$ (Fig. 1).

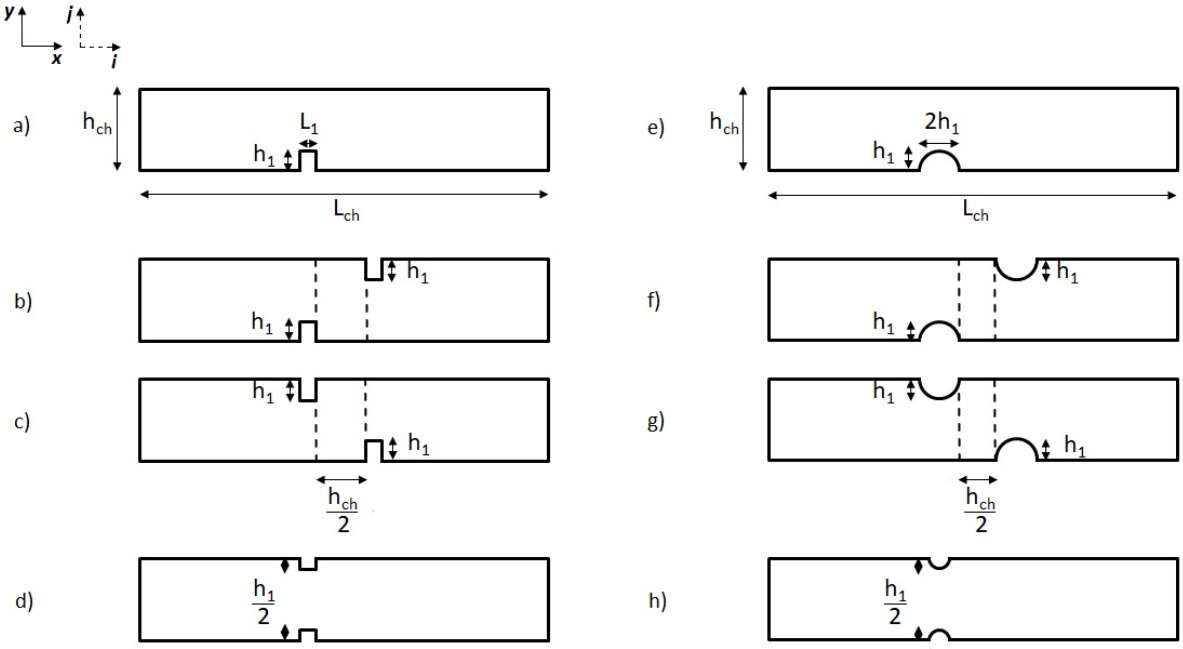

Fig. 1 Schematic illustration of the investigated channel geometries with obstacles ($h_1 = h_{ch}/6$). The analysis on models a, d, e and h is presented in the Results Section. Coordinates (*i, j*) correspond to the logical coordinates useful for the computational analysis

The analytical solution of the fluid motion in the microchannel without obstacles can be easily obtained from Navier-Stokes equations. In detail, for an incompressible, homogeneous, Newtonian fluid in steady-state laminar condition, the law of motion in the microchannel can be expressed as:

$$u_x = -\frac{1}{2\mu} \cdot \frac{dp}{dx} \cdot (y_0^2 - y^2) \quad (1)$$

where u_x is the velocity in axial (x, see Fig. 1) direction, μ the dynamic viscosity, p the pressure, y the general position in vertical direction (Fig. 1) and y_0 the coordinate of the microchannel wall, where velocity is equal to 0 (i.e. no-slip conditions).

The finite volume-based CFD commercial code Fluent (ANSYS Inc., USA) was adopted to solve the discretized governing equations of fluid motion in microchannels with obstacles. In detail, the Navier-Stokes equations in their discretized form and under steady-state laminar conditions were solved using a second order pressure discretization and a second order upwind momentum discretization scheme. The fluid was assumed to be isotropic, incompressible and Newtonian with a density value ρ equal to 998.2 [kg·m^{-3}] and a dynamic viscosity μ equal to 10^{-2} [kg·s·m^{-2}]. To ensure grid-independence of the solution, based on a mesh sensitivity analysis, quad-mesh with elements size of $1 \cdot 10^{-4}$ m was adopted. On average, the resulting computational grids consisted of 24000 elements and 24381 nodes. Two different

118 flow regimes, characterized by *Re* equal to 1 and 50, were simulated by applying Dirichlet
119 conditions at the inflow section of the microchannel geometry (in terms of flat velocity profile),
120 while the reference pressure Neumann boundary condition was imposed at the outflow section.
121 Walls were assumed to be rigid, and the no-slip condition was imposed.
122 The concept that a confined fluid in motion is an information carrier, and the parallel with a
123 communication system, was translated into a scheme where: (1) the fluid in the microchannel
124 is the carrier; (2) the inflow section (or more in general a section upstream of the channel
125 segment presenting obstacles) is the transmitter; (3) the outflow section (or more in general a
126 section downstream of the channel segment presenting obstacles) is the receiver; (4) the
127 difference in flow features between the two sections is the information transmitted. In this
128 regard, flow perturbations induced by the presence of obstacles can be regarded as the "noise"
129 affecting the system (Fig. 2). The channel without obstacles was considered as the reference
130 case, i.e. the case where the carrier (fluid) is not disturbed and the transmitted information is
131 not modified.
132

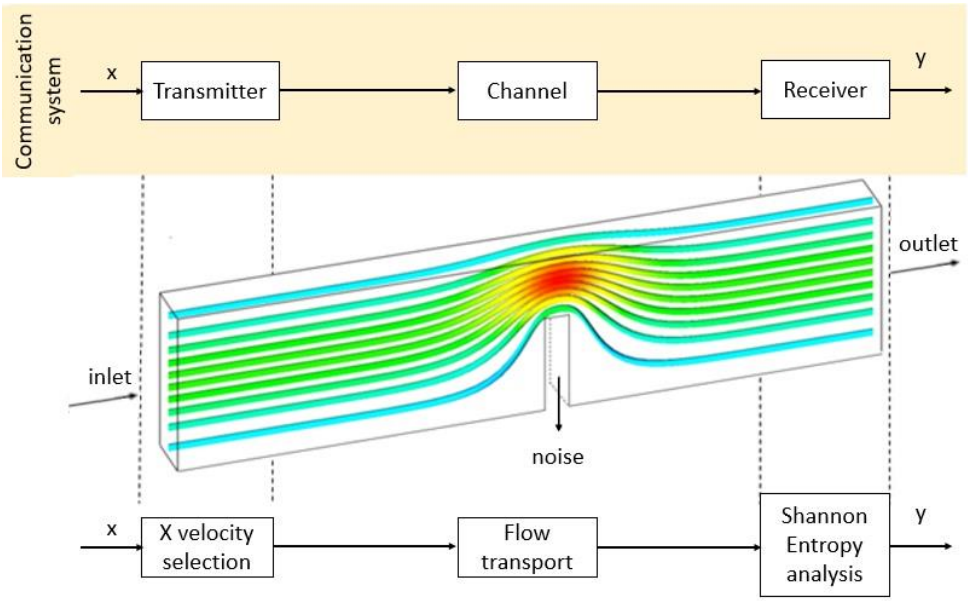

Fig. 2 Schematic illustration of the parallelism between a communication system and a fluidic system

Distilling in fluid mechanics terms, at the very low *Re* laminar flow regimes adopted in microfluid applications the streamlines deflection induced in the channel by the presence of an obstacle does represent a modification of the information content carried by the fluid at any channel location upstream of the obstacle. In the absence of obstacles, fluid streamlines will not be deflected, following a linear path; any obstacle capable to perturb the flow will deflect fluid streamlines and ultimately the carried information, in accordance with the conceptual model of Fig. 1. It is well known from the analytical solution of the laminar fluid motion in the channel without obstacles, that the flow field is characterized by streamlines parallel to the axis of the conduit (as well as to the channel's walls). The presence of an obstacle, even maintaining

laminar conditions, will perturb the flow with the consequence that streamlines will be deflected losing their parallelism. This behavior was translated building up a binary matrix, representative of the phenomena. To build up the representative binary matrix, here fluid velocity data from CFD simulations were considered (i.e. for each cell of the quad-mesh a value of velocity was extrapolated). Technically, a $N\,x\,M$ matrix $B_{i,j}^{x}$ was built:

$$B_{i,j}^{x} = \begin{bmatrix} b_{1,1} & \dots & b_{1,M-1} \\ \vdots & \ddots & \vdots \\ b_{N,1} & \dots & b_{N,M-1} \end{bmatrix} \quad (2)$$

with $i = \{1, \dots N\}$, where N is the number of grid cells in y direction, and $j = \{1, \dots M-1\}$, where M is the number of grid cells in x direction (Fig. 1). The binary elements $b_{i,j}$ of the matrix were calculated as follows:

$$b_{i,j} = \begin{cases} 1, & \frac{\bar{u}_{i,j}^{x}}{\bar{u}_{i,j-1}^{x}} \leq \zeta_{i,j} \\ 0, & otherwise \end{cases} \quad (3)$$

where $\bar{u}_{i,j}^{x}$ and $\bar{u}_{i,j-1}^{x}$ are the values of the x-component of the velocity at grid cell location (i, j) and (i, j-1), respectively. The threshold values $\zeta_{i,j}$ for matrix $B_{i,j}^{x}$ binarization were set according to:

$$\zeta_{i,j} = \frac{\bar{u}_{i,j}^{num.}}{\bar{u}_{i,j-1}^{num.}} - \frac{\bar{u}_{i,j}^{ana.}}{\bar{u}_{i,j-1}^{ana.}} = 0 \quad (4),$$

and depend on the results of CFD analysis and Eq. (1). From this equation, $\bar{u}_{i,j}^{num.}$ and $\bar{u}_{i,j}^{ana.}$ are the CFD and the analytical velocity values in x direction at grid cell location (i, j), and $\bar{u}_{i,j-1}^{num.}$ and $\bar{u}_{i,j-1}^{ana.}$ are the CFD and the analytical velocity values in x direction at grid cell location (i, j-1), respectively.

Here the SE was employed to quantify the level of interaction between fluid flow and the obstacles in the microchannel, intended as the level of streamlines deflection with respect to the microchannel without obstacles, binarized according to matrix $B_{i,j}^{x}$. By definition, the formulation of the SE is given by:

$$SE(X_i) = -P(X_i)\ log_2\ P(X_i) \quad (5),$$

where X_i is a discrete random variable with possible values $\{X_1, \ldots, X_n\}$ and $P(X_i)$ is the probability distribution of X_i. Theoretically, an increase of entropy corresponds to a loss in information content. In this study, the SE was evaluated according to:

$$SE = -P_i\ log_2\ P_i \quad (6)$$

where P_i is given by:

$$P_i = \frac{\sum_1^j b_{i,j}}{N} \quad (7)$$

Based on Eqs. (6) and (7), the SE ranges between zero (i.e. no information lost or, for the specific application, no distortion of fluid streamlines) and one (i.e. all the information carried

177 by the fluid lost due to the disruption of the flow field as a consequence of its interaction with
178 obstacles in the microchannel).
179
180 ## 3 Results
181 The analysis was extended to all the microchannels with different obstacles geometry and
182 number summarized in Fig. 1. As first explanatory example, the SE values computed along two
183 cross-sections (proximal and distal to the obstacle, respectively) of the two microchannels with
184 single obstacles of rectangular and semicircular shape, at two different *Re* numbers (1 and 50),
185 are presented in Fig. 3. At $Re = 1$, as expected, moderate differences are highlighted by the SE
186 both between the upstream and downstream sections (flow field distortion consequence of the
187 presence of the obstacle) and between the two microchannels (consequence of the different
188 shape of the obstacles). Marked differences in SE distribution (and in absolute values as well)
189 along the cross-sections emerge at $Re = 50$ (Fig. 3): as expected, the presence of the rounded
190 (semicircular) obstacle, which is expected to distort fluid streamlines less than the obstacle
191 with rectangular shape, modifies trans-obstacle SE values markedly less than the rectangular
192 single obstacle (the semicircular shape maintains almost unaltered the SE of the system even
193 increasing the inertial effects by one order of magnitude, as stated by the *Re*). The results of Fig.

194 3 confirm the capability of the SE of discriminating between obstacle shapes, properly

195 capturing thermodynamically-induced variations in the microchannel system.

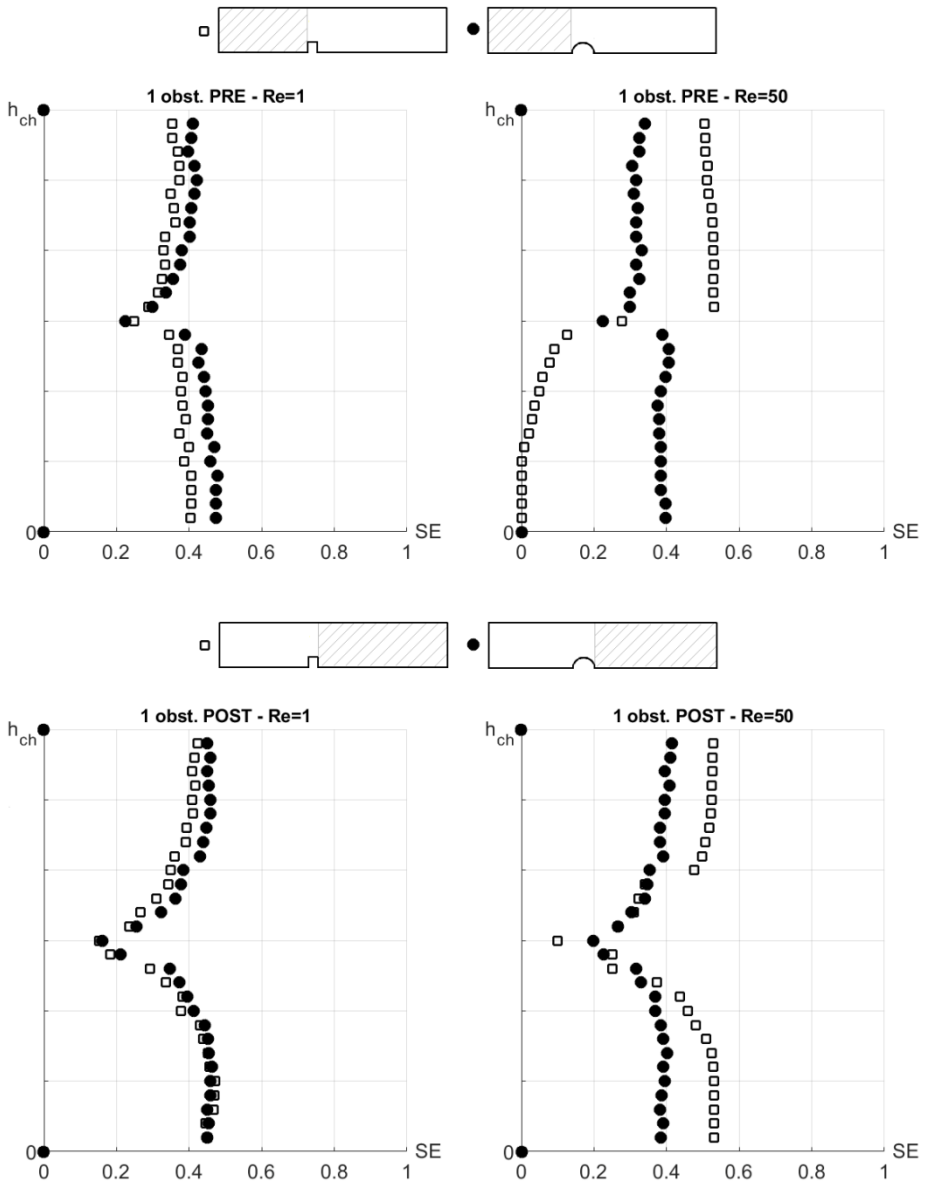

196

197 **Fig. 3** SE computed on two cross-sections (proximal to the obstacle, upper panel; distal to the obstacle,

198 lower panel) of two microchannels presenting single obstacles with different shape (rectangular and

199 semicircular), at two different *Re* (1 and 50). h_{ch} is the general height of the channel

200 Figure 3 also highlights an expected lack of symmetry (more pronounced at $Re = 50$) in the SE
201 cross-sectional distribution, reflecting the absence of geometrical and fluid dynamical
202 symmetry in the two microchannels with single obstacles. In this regard, the second
203 explanatory example of Fig. 4 reports the SE values computed along two cross-sections
204 (proximal and distal to the obstacle, respectively) of the two microchannels presenting
205 obstacles with rectangular and semicircular shape, symmetrically located with respect to the
206 microchannel axis. In this case, the cross-sectional SE distributions: (1) confirm the capability
207 of capturing the different influence of the shape of the obstacle in the flow field, with marked
208 differences related to the obstacle shape clearly evident also at $Re = 1$; (2) adequately reflect
209 the presence of a geometrical (and fluid dynamical) symmetry of the microchannel system.
210 Summarizing, the cross-sectional distributions of Figs. 3 and 4 clearly demonstrate that SE
211 is an indirect measure of the impact that obstacles with different shape and configuration have
212 on the microchannel fluid dynamics, suggesting that SE can be adopted to *a posteriori*
213 discriminate the shape of obstacles (e.g. cultured cells in biomicrofluidic applications) in
214 systems without optical access. This is like to say that SE can be used as a sort of *fingerprint*
215 that specific obstacles leave on fluid streamlines, depending upon their shape, configuration
216 and fluid dynamics conditions (as defined by the Reynolds' number).

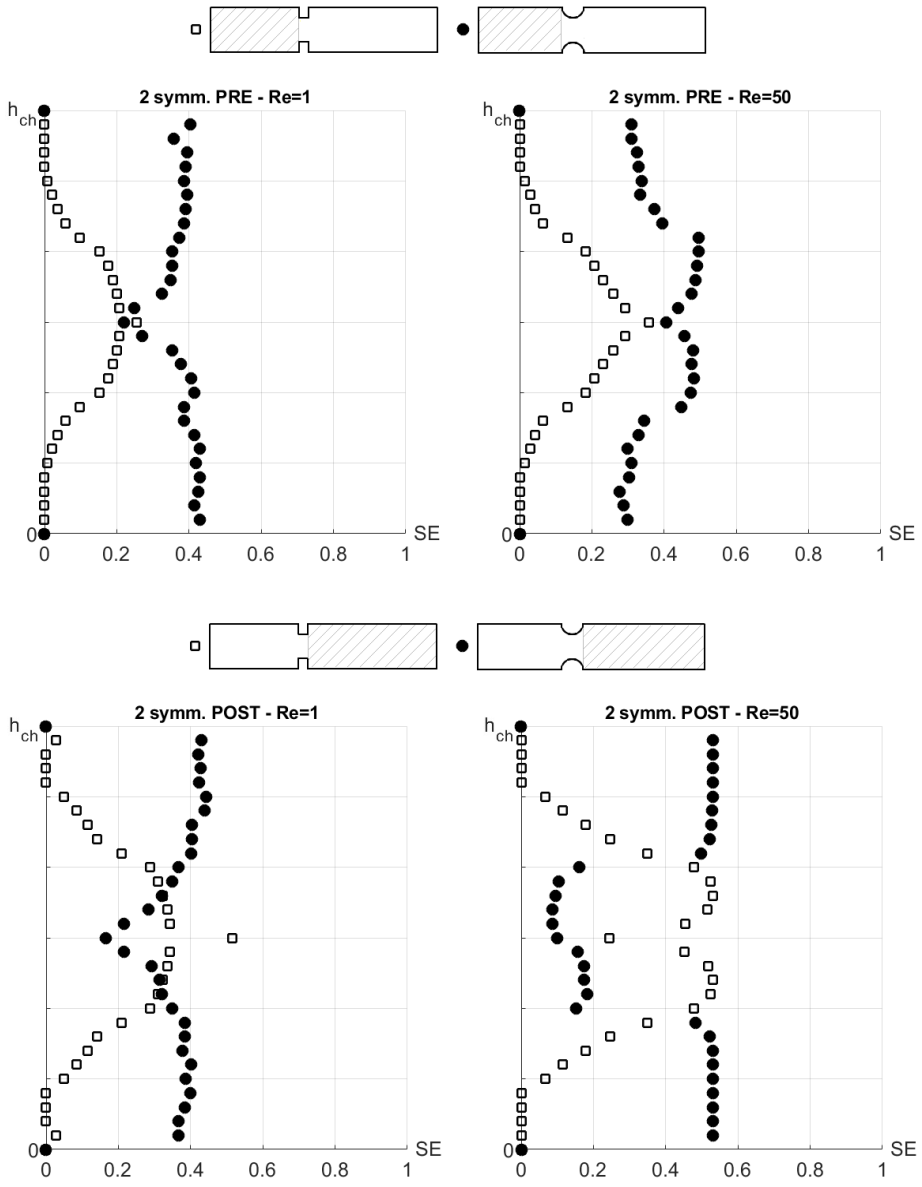

Fig. 4 SE computed on two cross-sections (proximal to the obstacle, upper panel; distal to the obstacle, lower panel) of two microchannels presenting obstacles with rectangular and semicircular shape, at *Re* = 1 and 50. Obstacles are symmetrically located with respect to the axis of the microchannels. h_{ch} is the general height of the channel.

In order to check for the robustness of SE with respect to the CFD grid cardinality (i.e. the number of nodes considered for the SE calculation), a sensitivity analysis was carried out where nodes were decimated. Technically, the average value of the SE was calculated considering the entire microchannel fluid domain as follows: (1) considering the 100% of the mesh grid elements; (2) considering only 50% of the mesh grid elements; (3) averaging the velocity values of two adjacent mesh grid elements. The percentage differences among the average SE values, summarized in Fig. 5 for microchannels with four different semicircular shape obstacle configurations, clearly show that a substantial reduction (50%) in the number of mesh grid elements weakly influences SE evaluation (with differences lower than 6%).

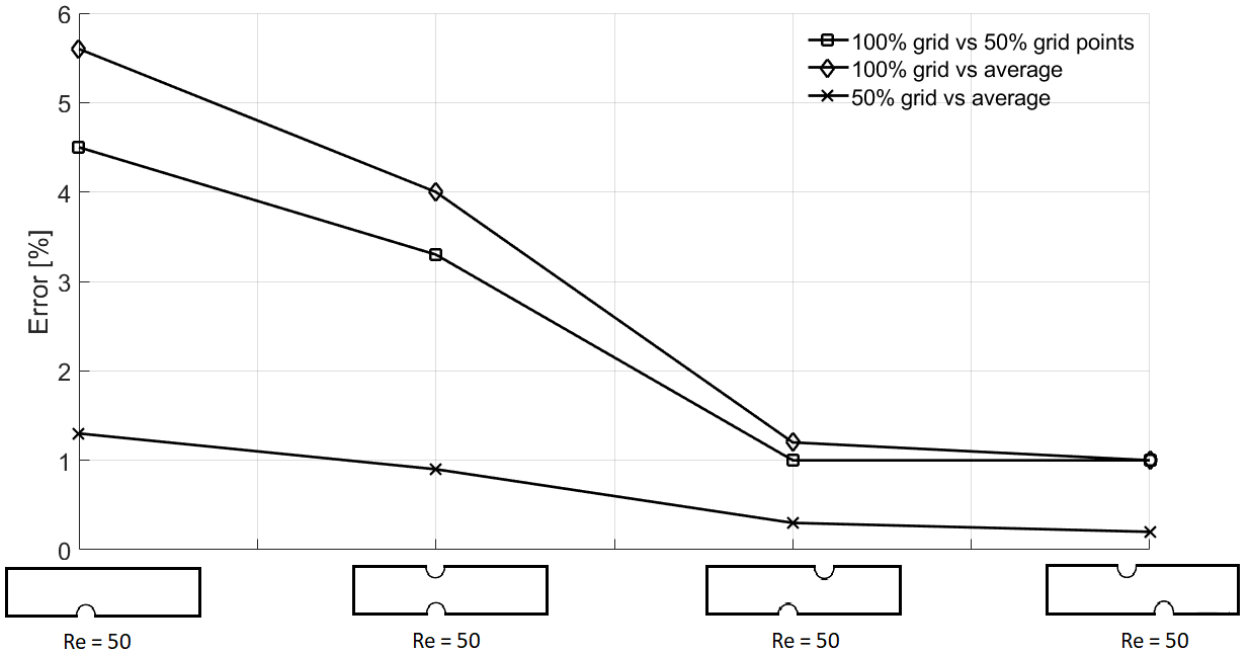

Fig. 5 Impact of the number of mesh grid elements on microchannel average SE values. The analysis was carried out considering the 100% and the 50% of the mesh grid elements, as well as averaging the

velocity values of two adjacent mesh grid elements. The results refer to four microchannels with different configurations of semicircular obstacles

4 Conclusions

In this study the fluid dynamics in microchannels with obstacles was investigated using the concept of entropy, here approached in a different way compared to the present state-of-the-art (Camesasca et al. 2006, Pozo et al. 2017, Rocha et al. 2008). The analysis suggests that a quantity linked to entropy, SE, is capable to discriminate among different shapes and configurations of obstacles within a microchannel. In the microfluidic field the capability to infer presence and configuration of obstacles in microsystems from SE differences between inflow and outflow sections could allow to monitor e.g. cells shape and growth in microbioreactors, as well as mixing of species in the microsystem itself. Applications other than biomicrofluidics, where fluid streamlines entropy can be employed to describe the physics within the microsystem just looking at SE input and output variations are manifold, ranging from microelectronics to chemistry (Ghaneifar et al. 2021, Shahsavar et al. 2020, Khalid et al. 2021). In this sense, the here presented results represent a starting point for future

dedicated applications where the extraction of information on the processes occurring inside a not accessible system is critical.

Integrating statistical mechanics with information theory, in the long run will allow to establish a clearly distinguishable link between thermodynamics perturbation of a system and the level of interaction of the individual elements of which a system is made.

Conflicts of interest

The authors declare that they have no competing interests.

References

Ali HM (2020) Recent advancements in PV cooling and efficiency enhancement integrating phase change materials based systems – A comprehensive review. Sol Energy 197:163–198. https://doi.org/10.1016/j.solener.2019.11.075

Bilen K, Yapici S (2002) Heat transfer from a surface fitted with rectangular blocks at different orientation angle. Heat Mass Transfer 38:649–655. https://doi.org/10.1007/s002310100275

267 Camesasca M, Kaufman M, Manas-Zloczower I (2006) Quantifying fluid mixing with the
268 Shannon entropy. Macromol Theory Simul 15:595–607.
269 https://doi.org/10.1002/mats.200600037
270 Chen C-Y, Su J-H, Ali HM, Yan W-M, Amani M (2020) Effect of channel structure on the
271 performance of a planar membrane humidifier for proton exchange membrane fuel cell. Int
272 J Heat Mass Transfer 163:120522.
273 https://doi.org/10.1016/j.ijheatmasstransfer.2020.120522
274 Cox SJ (2015) Simulations of bubble division in the flow of a foam past an obstacle in a narrow
275 channel. Colloids Surf, A 473:104–108. https://doi.org/10.1016/j.colsurfa.2014.10.038
276 Eijkel JCT, van den Berg A (2005) Nanofluidics: what is it and what can we expect from it?
277 Microfluid Nanofluid 1:249–267. https://doi.org/10.1007/s10404-004-0012-9
278 Ghaneifar M, Raisi A, Talebizadehsardari P (2021) Mixed convection heat transfer of Al_2O_3
279 nanofluid in a horizontal channel subjected with two heat sources. J Therm Anal Calorim
280 143:2761–2774. https://doi.org/10.1007/s10973-020-09887-2
281 Ikeda K, Matsumoto K (1989) Information theoretical characterization of turbulence. Phys Rev
282 Lett 62:2265–2268. https://doi.org/10.1103/PhysRevLett.62.2265

283 Khalid SU, Babar H, Ali HM, Janjua MJ, Ali MA (2021) Heat pipes: progress in thermal
284 performance enhancement for microelectronics. J Therm Anal Calorim 143:2227–2243.
285 https://doi.org/10.1007/s10973-020-09820-7
286 Khasanov NA (2011) Acoustic oscillations of a gas near nested thin-walled cylindrical obstacles
287 in a channel. J Appl Mech Tech Phys 52:577–584.
288 https://doi.org/10.1134/S0021894411040109
289 Merdasi A, Ebrahimi S, Moosavi A, Shafii MB, Kowsary F (2018) Simulation of a falling droplet
290 in a vertical channel with rectangular obstacles. Eur J Mech B Fluids 68:108–117.
291 https://doi.org/10.1016/j.euromechflu.2017.11.002
292 Pennella F, Mastrangelo F, Gallo D, Massai D, Deriu MA, Falvo D'Urso Labate G, Bignardi C,
293 Montevecchi F, Morbiducci U (2010) A survey of microchannel geometries for mixing of
294 species in biomicrofluidics. In: Dias R, Lima R, Martins AA, Mata TM (eds.) Single and two-
295 phase flows on chemical and biomedical engineering, 1st edn. Bentham Science Publishers,
296 Sharjah, pp 548–578. https://doi.org/10.2174/978160805295011201010548
297 Pennella F, Rossi M, Ripandelli S, Rasponi M, Mastrangelo F, Deriu MA, Ridolfi L, Kähler CJ,
298 Morbiducci U (2012) Numerical and experimental characterization of a novel modular

299 passive micromixer. Biomed Microdevices 14:849–862. https://doi.org/10.1007/s10544-
300 012-9665-4
301 Pozo JM, Geers AJ, Villa-Uriol M-C, Frangi AF (2017) Flow complexity in open systems:
302 interlacing complexity index based on mutual information. J Fluid Mech 825:704–742.
303 https://doi.org/10.1017/jfm.2017.392
304 Rocha LB, Adam RL, Leite NJ, Metze K, Rossi MA (2008) Shannon's entropy and fractal
305 dimension provide an objective account of bone tissue organization during calvarial bone
306 regeneration. Microsc Res Tech 71:619–625. https://doi.org/10.1002/jemt.20598
307 Sajjad U, Sadeghianjahromi A, Ali HM, Wang C-C (2020) Enhanced pool boiling of dielectric and
308 highly wetting liquids - a review on enhancement mechanisms. Int Commun Heat Mass
309 Transfer 119:104950. https://doi.org/10.1016/j.icheatmasstransfer.2020.104950
310 Shahsavar A, Ali HM, Mahani RB, Talebizadehsardari P (2020) Numerical study of melting and
311 solidification in a wavy double-pipe latent heat thermal energy storage system. J Therm
312 Anal Calorim 141:1785–1799. https://doi.org/10.1007/s10973-020-09864-9
313 Shannon CE (1948) A mathematical theory of communication. Bell Syst Tech J 27:379–423.
314 https://doi.org/10.1002/j.1538-7305.1948.tb01338.x

315 Sözen A, Filiz Ç, Aytaç İ, Martin K, Ali HM, Boran K, Yetişken Y (2021) Upgrading of the
316 performance of an air-to-air heat exchanger using graphene/water nanofluid. Int J
317 Thermophys 42:35. https://doi.org/10.1007/s10765-020-02790-w
318 Tariq HA, Anwar M, Malik A, Ali HM (2020) Hydro-thermal performance of normal-channel
319 facile heat sink using TiO_2-H_2O mixture (Rutile-Anatase) nanofluids for microprocessor
320 cooling. J Therm Anal Calorim. https://doi.org/10.1007/s10973-020-09838-x
321 Wang X, Li C, Zhang Y, Ding W, Yang M, Gao T, Cao H, Xu X, Wang D, Said Z, Debnath S, Jamil M,
322 Ali HM (2020) Vegetable oil-based nanofluid minimum quantity lubrication turning:
323 Academic review and perspectives. J Manuf Processes 59:76–97.
324 https://doi.org/10.1016/j.jmapro.2020.09.044
325 Yojina J, Ngamsaad W, Nuttavut N, Triampo D, Lenbury Y, Kanthang P, Sriyab S, Triampo W
326 (2010) Investigating flow patterns in a channel with complex obstacles using the lattice
327 Boltzmann method. J Mech Sci Technol 24:2025–2034. https://doi.org/10.1007/s12206-
328 010-0712-x